SECURITY CL

AD-A266 827

DOCUMENTATION PAGE

1a. REPORT

1b. RESTRICTIVE MARKINGS

2a. SECURITY CLASSIFICATION AUTHORITY

3. DISTRIBUTION/AVAILABILITY OF REPORT
Approved for public release; distribution is unlimited

2b. DECLASSIFICATION/DOWNGRADING SCHEDULE

4. PERFORMING ORGANIZATION REPORT NUMBER(S)
NMRI 93-47

5. MONITORING ORGANIZATION REPORT NUMBER(S)

6a. NAME OF PERFORMING ORGANIZATION
Naval Medical Research Institute

6b. OFFICE SYMBOL (If applicable)

7a. NAME OF MONITORING ORGANIZATION
Naval Medical Command

6c. ADDRESS (City, State, and ZIP Code)
8901 Wisconsin Avenue
Bethesda, MD 20889- 5607

7b. ADDRESS (City, State, and ZIP Code)
Department of the Navy
Washington, DC 20372-5120

8a. NAME OF FUNDING/SPONSORING ORGANIZATION
Naval Medical Research & Development Comman

8b. OFFICE SYMBOL (If applicable)

9. PROCUREMENT INSTRUMENT IDENTIFICATION NUMBER

8c. ADDRESS (City, State, and ZIP Code)
8901 Wisconsin Avenue
Bethesda, MD 20889- 5606

10. SOURCE OF FUNDING NUMBERS

PROGRAM ELEMENT NO.	PROJECT NO.	TASK NO.	WORK UNIT ACCESSION NO.
62233N	MM33P30	004.1050	DN249500

11. TITLE (Include Security Classification)
Contribution of tissue lipid to long xenon residence times in muscle

12. PERSONAL AUTHOR(S)
Novotny JA, Parker EC, Survanshi SS, Albin GW, Homer LD

13a. TYPE OF REPORT	13b. TIME COVERED	14. DATE OF REPORT (Year, Month, Day)	15. PAGE COUNT
journal article	FROM _____ TO _____	1993	8

16. SUPPLEMENTARY NOTATION
Reprinted from: Journal of Applied Physiology 1993 Vol.74 No.5 pp. 2127-2134

17. COSATI CODES			18. SUBJECT TERMS (Continue on reverse if necessary and identify by block number)
FIELD	GROUP	SUB-GROUP	inert gas; decompression modeling; mathematical model

19. ABSTRACT (Continue on reverse if necessary and identify by block number)

20. DISTRIBUTION/AVAILABILITY OF ABSTRACT
☒ UNCLASSIFIED/UNLIMITED ☐ SAME AS RPT ☐ DTIC USERS

21. ABSTRACT SECURITY CLASSIFICATION
Unclassified

22a. NAME OF RESPONSIBLE INDIVIDUAL
Phyllis Blum, Librarian

22b. TELEPHONE (Include Area Code)
(301) 295-2188

22c. OFFICE SYMBOL
MRL/NMRI

DD FORM 1473, 84 MAR

83 APR edition may be used until exhausted
All other editions are obsolete.

SECURITY CLASSIFICATION OF THIS PAGE
UNCLASSIFIED

DISCLAIMER NOTICE

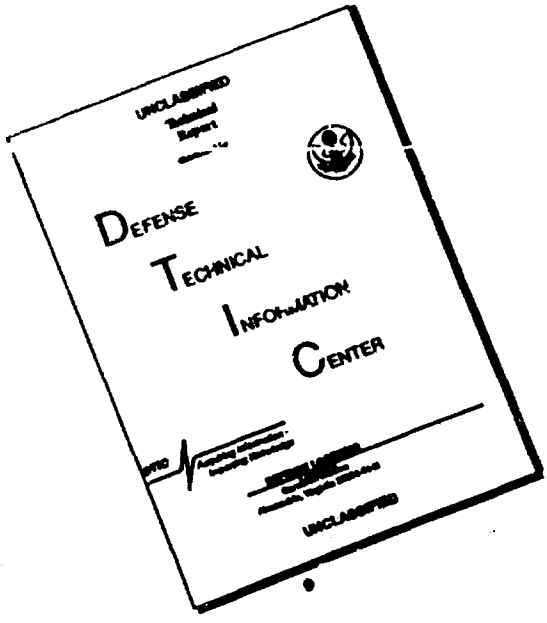

THIS DOCUMENT IS BEST QUALITY AVAILABLE. THE COPY FURNISHED TO DTIC CONTAINED A SIGNIFICANT NUMBER OF PAGES WHICH DO NOT REPRODUCE LEGIBLY.

Contribution of tissue lipid to long xenon residence times in muscle

J. A. NOVOTNY, E. C. PARKER, S. S. SURVANSHI, G. W. ALBIN, AND L. D. HOMER
Naval Medical Research Institute, Bethesda, Maryland 20889–5055

NOVOTNY, J. A., E. C. PARKER, S. S. SURVANSHI, G. W. ALBIN, AND L. D. HOMER. *Contribution of tissue lipid to long xenon residence times in muscle.* J. Appl. Physiol. 74(5): 2127–2134, 1993.—Experiments demonstrate that the mean residence time of an inert gas in tissue is longer than that predicted by a single-compartment model of gas exchange. Also the relative dispersion (RD, the standard deviation of residence times divided by the mean) is 1 according to this model, but RDs in real tissues are closer to 2, suggesting that a multiple-compartment model might be more accurate. The residence time of a gas is proportional to its solubility in the tissue. Although the noble gases in particular are 10 times more soluble in lipid than in nonlipid tissues, models of gas exchange generally do not incorporate measurements of the lipid in tissue, which may lead to error in the predicted gas residence times. Could a multiple-compartment model that accounts for the lipid in tissue more accurately predict the mean and RD of gas residence times? In this study, we determined the mean and RD of Xe residence times in intact and surgically isolated muscles in a canine model. We then determined the lipid content and the perfusion heterogeneity in each tissue, and we used these measurements with a multiple-compartment model of gas exchange to predict the longest physiologically plausible Xe residence times. Even so, we found the observed Xe mean residence times to be twice as long as those predicted by the model. However, the predicted RDs were considerably larger than the observed RDs. We conclude that lipid alone cannot account for the residence times of Xe in tissue and that a multiple-compartment model is not an accurate representation of inert gas exchange in tissue. A more accurate model will need to account for other features in the tissue, such as diffusion of gas between vessels and structures with heterogeneous solubility.

inert gas; mathematical model; decompression modeling

THE SIMPLEST MODEL of the exchange of dissolved inert gases between blood and tissue considers the tissue as a single well-mixed compartment. However, empirical studies on inert gas exchange find that the mean residence time observed in the tissue is nearly always longer than that predicted by the model (2, 7, 9). According to the single-compartment model, the gas uptake and elimination curve is a single-exponential function, and the mean residence time of the gas is equal to λ/F, where the tissue-blood partition coefficient (λ) is the ratio of the average solubility of the gas in the tissue to its solubility in the blood and F is the blood flow rate per unit volume. The relative dispersion (RD, the standard deviation of gas residence times divided by the mean) of a single-exponential process is 1, but RDs observed in tissues are closer to 2 (12, 15), indicating a wider distribution of residence times. A multiple-compartment model can account for RDs >1 and so may be a more accurate representation of inert gas exchange in tissue. However, we previously found that such a model can account for only a small fraction of the observed RD when only the heterogeneous blood flow in the tissue and an assumed constant value for λ are considered (6). Is another model required, or is the multiple-compartment model in error because of incomplete information about the parameters F and λ?

One previous study on Xe exchange in skeletal muscle (15) attributed the unexpectedly long Xe elimination times to bits of lipid that were observed on visual inspection of the tissue. The residence time of an inert gas is proportional to its solubility in the tissue, and the noble gases in particular are ~10-fold more soluble in lipid than in nonlipid tissues (17). The lipid content of muscle tissue is variable (4, 8), so tissues with above-average amounts of lipid would have longer gas residence times than would be predicted considering only the average published values of gas solubility in tissue. How much lipid would be necessary to account for the Xe residence times observed in tissues?

In this study, we tested the hypothesis that the lipid present in a sample of normal canine muscle and subcutaneous tissues can account for the mean residence time of Xe gas. We substituted values for λ into a multiple-compartment model on the basis of the measured lipid content of the tissue and biased the model to estimate the longest plausible mean residence times. We also estimated the effect of the lipid on the RD of residence times in the presence of heterogeneous tissue blood flow rates.

METHODS

We studied eight dogs (*Canis familiaris*, 1–2 yr old, male, 13–26 kg) anesthetized with pentobarbital sodium and mechanically ventilated. The methods were similar to those described previously (13). Only modifications to those techniques are described here.

The experimental protocol for this project was reviewed by the institutional Animal Care and Use Committee and certified as conforming to guidelines in Institute for Laboratory Resources, National Research Council "Guide for the Care and Use of Laboratory Animals" (DHHS publ. 86–33).

Xe Administration

The dogs breathed from a closed-circuit ventilator. At the start of the experiment, ^{133}Xe gas was injected into

the ventilator to establish a step increase in the concentration of ^{133}Xe in the inspired air, which was then maintained constant for 2.5 h of Xe uptake by continuously adding ^{133}Xe and monitoring the radioactivity of the inspired limb of the ventilator circuit. At the end of the Xe uptake period, the ventilator was suddenly switched to open-circuit breathing for 2.5 h of Xe elimination.

Tissue Site Preparation

The skin and subcutaneous tissues may contain considerably more lipid than the underlying muscle tissue. We studied both intact hindleg muscles and muscles stripped of the overlying nonmuscle tissues to increase the range of lipid contents of our sampled tissues. We randomly selected either the right or the left calf muscle for surgical isolation. The skin, subcutaneous fat, and connective tissues were lifted by blunt dissection and retracted, and the isolated muscle was covered in 0.6-mm-thick plastic wrap (Saran) and suffused with 0.9% saline at 37°C. If we assume that the plastic wrap (product code 06042, Dow Plastics, Dow Chemical) is no more permeable to Xe than to N_2, we can expect <1/800th of the Xe gas delivered to the tissue in blood to be lost through this surface, a small loss that would not be reliably detected with our system. The other leg was left intact. The surface temperature of the isolated muscle and the subcutaneous temperature of the intact side (via a 3-mm incision in the skin) were continuously monitored with 2-mm probes (Digitec, Dayton, OH). Similar temperatures were maintained on both sides.

Xe Detection

Using 9-mm-diam cylindrical detectors containing CdTe semiconductors (RMD, Watertown, MA), we recorded the radioactivity of ^{133}Xe as a function of time. Using 8-mm-thick barrel-shaped lead collimators, we shielded the detectors. We aligned the collimators visually over the intact and the isolated muscle preparations, excluding the bone from the field of view of the detector. We simultaneously recorded the background radioactivity with a detector positioned midway between the two detectors over the tissues. The background radioactivity is time dependent, reaching ~500 cpm at the peak of an experiment compared with a typical tissue signal of 10,000 cpm. To simulate the secondary radiation generated by the ambient radioactivity and the detected tissues (15), beneath the background detector we positioned a water-filled plastic cone with the same dimensions as the detector field of view.

We subtracted the background at each time point from the tissue data. To smooth the fluctuations in difference of two random variables, we first fitted curves to the background data and took the net tissue signal as the difference between the raw tissue data and the smoothed background.

Measuring the Tissue Layer Thickness

We measured the thicknesses of the muscle and nonmuscle tissues of the intact side at the end of each experiment. This information is important, because the skin and subcutaneous tissues are closer to the detector and therefore contribute more efficiently to the detected signal than the more distant muscle tissue. The digital calipers had a resolution of 0.01 mm (Ultra-cal II, Fowler, Westmont, IL), which resulted in a standard deviation of <1 mm on repeated measurements. The APPENDIX explains how we used these measurements to estimate the contribution of the nonmuscle tissue to the total detected Xe radioactivity of the intact side.

Measuring the Tissue Blood Flow

To determine an average blood flow for each tissue piece during the 5-h Xe exchange period, we used radioactive microspheres to make four equally spaced measurements. The first was at the beginning of Xe uptake, with two more at 100-min intervals, and the last was at the end of the Xe elimination period. We used 15-μm microspheres labeled with ^{51}Cr, ^{95}Nb, ^{103}Ru, or ^{141}Ce (NEN, Dupont, Wilmington, DE) and injected them in aliquots of 2×10^5 microspheres/kg in 10 ml of 0.9% saline over 15 s through a catheter placed in the left ventricle via the left common carotid artery. Reference blood samples were simultaneously withdrawn from a brachial artery catheter at 2 ml/min for 2 min and accompanied by an equal-volume infusion of Dextran-70 into a pulmonary artery catheter.

At the end of the experiment, using a scalpel, we removed the tissues in the field of view of the Xe detectors. We then manually separated the tissues of the intact side into muscle and nonmuscle portions. The average weights of the muscle and the nonmuscle tissues were 30 and 10 g, respectively. We then cut the tissues into 1-g pieces with a scalpel, weighed them, and placed them in plastic tubes for counting in a four-channel scintillation detector (LKB Wallac, Gaithersburg, MD), which enabled the estimation of the blood flow rates at the four times.

The average tissue blood flow over the four measurements for the jth piece (F_j, $ml \cdot min^{-1} \cdot ml^{-1}$) was calculated as

$$F_j = 1/4 \sum_{k=1}^{4} \frac{R_{jk}}{R_{T\,k}} W \qquad (1)$$

where R_{jk} is the radioactivity for the kth measurement of the jth tissue piece, $R_{T\,k}$ is the radioactivity of the arterial reference sample, and W is the reference withdrawal rate (ml/min). The volume of the tissue was calculated as described below.

Measuring the Tissue Lipid

After counting the microsphere radioactivity, we pooled the tissue pieces into their three original groupings (muscle from the isolated side, muscle from the intact side, and nonmuscle from the intact side) and extracted the lipid. The limitations of the lipid extraction method (1) prevented measurement of the lipid content of the individual 1-g pieces of tissue. The lipid contents of our tissue samples ranged from 0.5 to 7.5 g. We tested the accuracy of the method by extracting amounts of corn oil in the same range as our tissue lipid values. We found that the oil was accurately recovered in this range, with a coefficient of variation of 4% on replicate samples. Using

densities of 0.9 for the lipid and 1.1 for the residual nonlipid material (11), we estimated the volumes of the tissue samples according to the lipid fractions and the measured weights.

Analysis

We compared the observed means and RDs of Xe residence times with the predictions of a model that accounts for the lipid and the blood flow of the tissue.

Observed Xe kinetics. The Xe radioactivity-time curves less the smoothed background were fitted with sums of exponentials, as described previously (12). The mean and the RD of residence times were then calculated from the parameters of the least-squares fit.

Predicted Xe kinetics. The model includes variables to represent both the lipid content and the blood flow heterogeneity of the tissue. For the intact side, we estimated the mean and the RD of Xe residence times as averages of the muscle and nonmuscle tissues weighted according to their volumes and relative positions beneath the detector (APPENDIX). The details of the model are outlined in *Eqs. 2–13.*

For each experiment, the tissue-sampling method yields several 1-g pieces of muscle and, on the intact side, muscle and nonmuscle tissue. Each 1-g piece was considered as a well-mixed compartment for the exchange of Xe between blood and tissue. The composite of tissue in the detector field of view was then modeled as a collection of n such compartments. The jth piece has an exponential time constant τ_j (minutes) that depends on the partition coefficient and the blood flow per unit volume, F_j

$$\tau_j = \frac{\lambda}{F_j} \tag{2}$$

The predicted Xe transfer function for the ith tissue is

$$h(t)_i = \sum_{j=1}^{n} \left(\frac{F_j}{F_T}\right)(1/\tau_j)\exp(-t/\tau_j) \tag{3}$$

with i = 1–3 representing the muscle tissue of the isolated side and the muscle and nonmuscle tissues of the intact side, respectively. F_T is the total of the F_j.

The predicted Xe mean residence time, the first moment about the origin ($E[t]_i$), is the flow-weighted average of the tissue pieces

$$E[t]_i = \sum_{j=1}^{n_L} \left(\frac{F_j}{F_T}\right)(\lambda_L V_j/F_j) + \sum_{j=n_L+1}^{n} \left(\frac{F_j}{F_T}\right)(\lambda_{NL} V_j/F_j) \tag{4}$$

where λ_{NL} and λ_L are the tissue-blood partition coefficients for the nonlipid and the lipid compartments, respectively, and n_L is the number of the tissue pieces considered as lipid. Although our lipid extraction method did not determine the lipid contents of the individual pieces, the mean residence time depends only on the total lipid content and the total blood flow, as explained below.

The tissues we harvested from the animals included muscle tissue and skin and subcutaneous nonmuscle tissue, for which the average published tissue-blood partition coefficients for Xe are 0.68 (17) and 0.87 (10), respectively. Our sampled tissues had a wide range of lipid contents. To account for this variability, we estimate λ for the tissues in each experiment according to their measured lipid contents. We assigned these published values of λ to the tissues having the lowest lipid contents of those sampled in all the experiments. We then accounted for the higher lipid contents of the tissues in all the other experiments by assigning λ_L = 9.8 (17) to the n_L pieces corresponding to the volume fraction of lipid in *Eq. 4.* This ensures that all the sampled tissues have average λ values at least as large as the published values and that the model estimates mean residence times as long as physiologically plausible.

How does the predicted mean residence time depend on the spatial arrangement of the lipid and the blood flow in the tissue? Summing the volumes to total volume (V_T) and rewriting *Eq. 4* in terms of the tissue lipid fraction (ω) show that the mean residence time depends only on the ratio of V_T to F_T and the weighted average of the λ_L and λ_{NL} but not on their location in the tissue

$$E[t]_i = \frac{V_T}{F_T}[\omega\lambda_L + (1-\omega)\lambda_{NL}] \tag{5}$$

We can use this expression to estimate the tissue-blood partition coefficient for each tissue as the weighted average of the lipid and nonlipid portions

$$\lambda_. = \omega\lambda_L + (1-\omega)\lambda_{NL} \tag{6}$$

where $\lambda_.$ is the average λ.

The predicted second moment about the origin ($E[t^2]$) of the distribution of Xe residence times is

$$E[t^2]_i = 2\sum_{j=1}^{n_L}\left(\frac{F_j}{F_T}\right)(\lambda_L V_j/F_j)^2 + 2\sum_{j=n_L+1}^{n}\left(\frac{F_j}{F_T}\right)(\lambda_{NL} V_j/F_j)^2 \tag{7}$$

which is used to calculate the variance and the RD.

The second moment, and so the RD, depends on the distribution of lipid and blood flow in the tissue. This can be shown by simplifying *Eq. 7* to

$$E[t^2]_i = 2\frac{\lambda_L}{F_T}\sum_{j=1}^{n_L} V_j\tau_j + 2\frac{\lambda_{NL}}{F_T}\sum_{j=n_L+1}^{n} V_j\tau_j \tag{8}$$

Because the tissue piece volumes (V_j) are similar in size, we can replace them with a standard volume (V_s) to simplify *Eq. 8* to

$$E[t^2]_i = 2\lambda_L\frac{V_s}{F_T}\sum_{j=1}^{n_L}\tau_j + 2\lambda_{NL}\frac{V_s}{F_T}\sum_{j=n_L+1}^{n}\tau_j \tag{9}$$

and then rearrange to obtain

$$E[t^2]_i = 2\frac{V_s}{F_T}\left(\frac{\lambda_L}{\lambda_{NL}}\sum_{j=1}^{n_L}\tau_j + \sum_{j=n_L+1}^{n}\tau_j\right) \tag{10}$$

Ideally, we would know λ for each of the n tissue pieces, but without this information we can at least determine the range of RDs possible within this model. Because $\lambda_L > \lambda_{NL}$, assigning the largest τ values (the lowest blood flows) in *Eq. 10* to the lipid portion maximizes the predicted RD, and assigning the smallest τ values to the lipid minimizes it. If the multiple-compartment model is accurate, the distribution of lipid and blood flows actually present in the tissue must lie between these two extremes. We first calculated the RDs by assuming that the lipid portion should be paired with the higher of the mea-

sured blood flows. We then made the same calculations under the assumption that lipid should receive the lower of the measured blood flows. We examined a third assumption that the lipid is evenly distributed among the tissue pieces by simplifying *Eq. 7* to

$$E[t^2]_i = 2\sum_{j=1}^{n}\left(\frac{F_j}{F_T}\right)(V_j/F_j)^2[\omega\lambda_L + (1-\omega)\lambda_{NL}] \quad (11)$$

We estimated the moments of the intact side as the weighted averages of the moments of the muscle and nonmuscle tissues. The first moment for the intact side is

$$E[t]_{23} = (1-\delta)E[t]_2 - (\delta)E[t]_3 \quad (12)$$

and the second moment is

$$E[t^2]_{23} = (1-\delta)E[t^2]_2 + (\delta)E[t^2]_3 \quad (13)$$

where δ, the weighting factor for the contribution of the nonmuscle layer to the detected Xe activity, is calculated from the measured tissue layer thicknesses, as described in the APPENDIX. Finally, the predicted variance is equal to $E[t^2] - (E[t])^2$, from which the RD is calculated as $(\text{variance}/\text{mean}^2)^{1/2}$.

Statistical Analysis

The number of exponential terms required to fit the Xe data was selected according to reductions in the residual error by use of an F test. The observed and predicted means and RDs were compared by calculating 95% confidence intervals.

RESULTS

Observed Xe Kinetics

A typical profile of inspired Xe radioactivity and the radioactivity detected in the tissue is shown in Fig. 1. We fitted the curves using an expression with two exponential terms. This expression fits the data well (Fig. 1). The estimates of the mean residence times had coefficients of variation of ≤3.5%, similar to previous results (12). Attempts at fitting with one exponential term produced visibly poorer fits, which were nearly always rejected as statistically less satisfactory than the two-exponential fits ($P < 0.05$). Attempts to fit three exponentials to the data produced statistically significant improvements over the two-exponential fits in only 2 of 16 cases. The mean residence times estimated from the three-exponential fits were similar to those obtained using two-exponential terms.

The observed mean residence times estimated for the intact side were longer than those estimated for the isolated muscles: 35.4 vs. 23.0 min (Table 1). The observed RDs were similar for the two sides: 1.61 for intact and 1.76 for isolated.

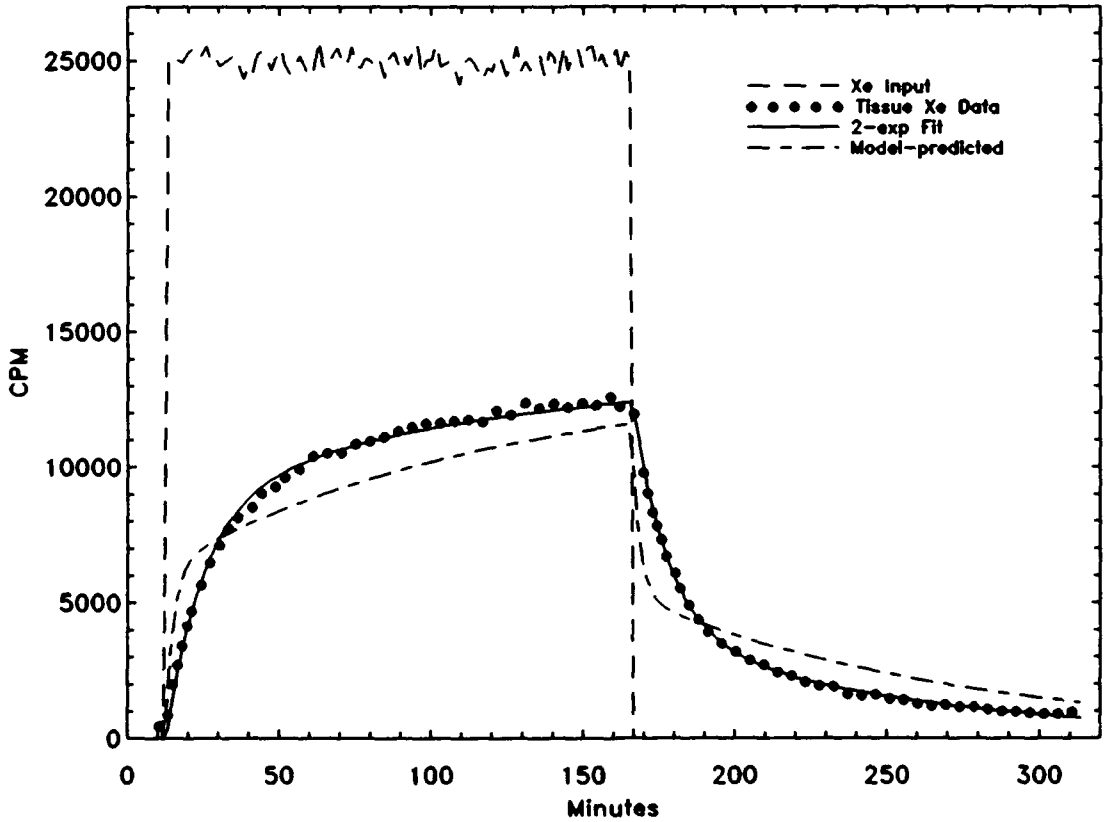

FIG. 1. Profiles of Xe radioactivity over time in inspired air (Xe input) and tissue (tissue Xe data) for isolated muscle in *expt 5* and 2-exponential fitted curve (2-exp fit). Predicted mean residence time was 5.3 min; observed mean residence time was 17.2 min. Also shown is tissue Xe curve predicted by multiple-compartment model, with lower perfusion rates assigned to lipid (model-predicted). Shapes of curves reflect differences between observed and predicted relative dispersions.

TABLE 1. *Observed and predicted Xe mean residence times*

Expt No.	Isolated		Intact	
	Observed	Predicted	Observed	Predicted
1	21.8±0.3	8.8	41.2±0.6	30.6
2	39.4±2.2	23.3	52.0±1.7	47.2
3	12.0±0.4	9.1	25.9±1.2	36.8
4	33.0±1.3	14.6	60.2±8.4	30.4
5	17.2±0.3	5.3	20.7±0.4	7.7
6	21.0±0.5	7.7	23.1±0.4	8.6
7	15.1±0.7	8.8	16.6±0.5	13.8
8	24.6±0.4	10.0	43.6±1.1	25.8
Avg	23.0	11.0	35.4	25.1

Values are means ± SD in minutes.

Predicted Xe Kinetics

The average vol/vol fraction of lipid in the isolated muscle was 6.0% (range 3.2–13%), similar to previously reported values (4, 8), and the average in the tissues of the intact side was 13% (range 3.4–35%). The corresponding average tissue-blood partition coefficients estimated using *Eq. 6* to account for the measured lipid were 0.98 (range 0.68–1.60) for the isolated muscle and 1.61 (range 0.73–3.60) for the intact side. The average blood flows were 9.5 ml · min^{-1} · 100 g^{-1} for the isolated muscle and 7.3 ml · min^{-1} · 100 g^{-1} for the intact side. The muscle tissue of the intact side was on average 2.8 cm thick, and the nonmuscle tissue was on average 0.4 cm thick. As a straight percentage, the nonmuscle tissue layers represented just 12.5% of the total thickness of the intact side. However, considering the locations of the tissues with respect to the detector and the geometry of the field of view of the detector, we estimate that the nonmuscle tissues contributed an average of 25% of the Xe signal recorded from the intact side (see APPENDIX).

The predicted mean residence times for the intact side were longer than those of the isolated muscles: 25.1 and 11.0 min, respectively (Table 1). With incorporation of the perfusion heterogeneity alone, the model predicted an average RD of only 1.16. Adding the effect of lipid increased the predicted RDs to 2.5–5. Pairing the lipid with the highest of the measured flows produced RDs of ~2.5, whereas pairing the lipid with the lowest flows increased the predicted RDs to ~5. Distributing the lipid evenly throughout the tissue produced intermediate values averaging ~3.

Observed vs. Predicted Kinetics

The observed mean residence times were on average twice as long as those predicted by the model for the isolated and the intact sides (95% confidence interval 1.6–2.3). This can be appreciated visually in the plots of the mean residence times shown in Fig. 2. The predicted mean residence times fall short of the line of equality in all but one case (*Expt 3, intact,* Table 1). The observed and predicted mean residence times are correlated (r = 0.87 for isolated, r = 0.69 for intact; $P < 0.05$).

Figure 3 summarizes the observed RDs and those predicted by the model. The observed RD of 1.68 is similar to previously reported values (12, 16). Incorporating the measured perfusion heterogeneity and a single constant λ for the tissue, ignoring the compositional heterogeneity, the model predicted an RD of only 1.16, which is not much larger than the RD of 1 for a well-mixed compartment. However, incorporating λ values to reflect the lipid content of the tissue increased the predicted RDs considerably. Distributing the lipid evenly among the heterogeneous perfusion rates produced an average RD of 3.34 (*Eq. 11*). We estimated the range of RDs possible under this model by pairing the lipid with the higher and with the lower of the measured blood flows (*Eq. 10*), which produced average RDs of 2.53 and 4.88, respectively.

DISCUSSION

Mean Residence Time

Lipid alone cannot account for the observed residence times of Xe in tissue. The mean residence times predicted by the present model were as long as physiologi-

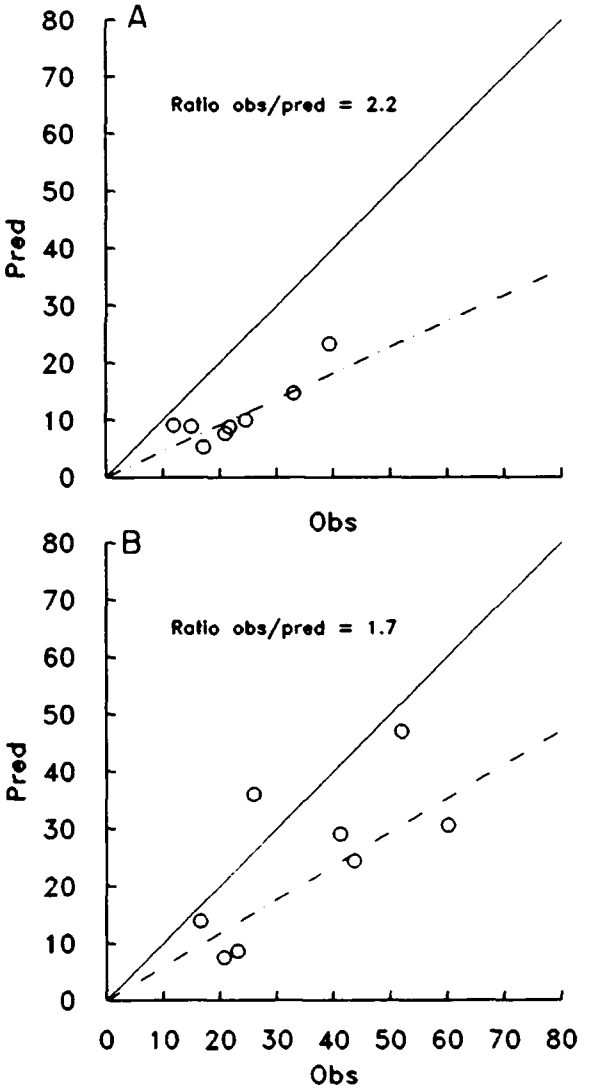

FIG. 2. Plot of observed (x-axis) vs. predicted (y-axis) mean residence times for isolated (*A*) and intact (*B*) muscles. In both cases, fitted regression (dashed) lines fall below (solid) line of equality, reflecting longer observed than predicted Xe residence times. Average ratios of observed to predicted mean residence times are 2.2 for isolated side and 1.7 for intact side.

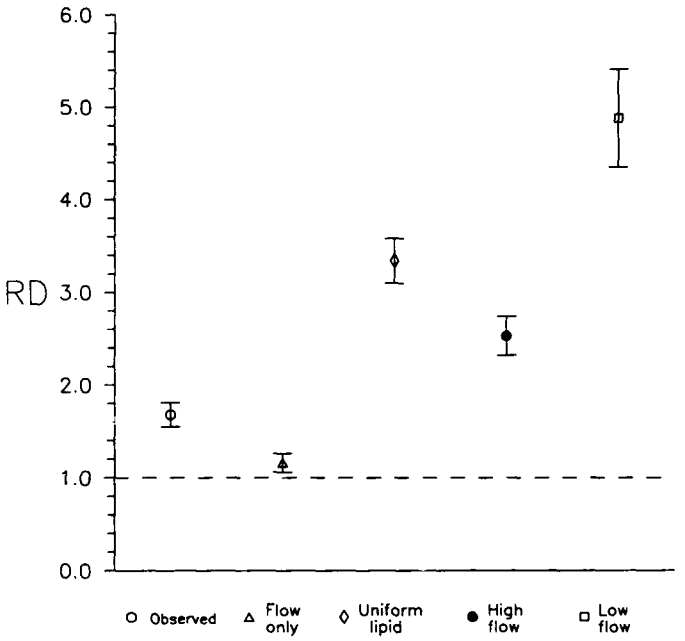

FIG. 3. Observed and predicted Xe relative dispersions (RDs), with 95% confidence intervals shown in parentheses. Average of observed RDs (Observed) was 1.68 (1.55–1.82). With incorporation of tissue blood flow heterogeneity alone (flow only), model predicted an RD of 1.16 (1.11–1.21). Including lipid evenly throughout tissue (uniform lipid) increased predicted RD to 3.34 (3.10–3.58). Pairing lipid with highest of measured blood flows (high flow) predicted an RD of 2.53 (2.32–2.74), whereas pairing with lowest flows (low flow) predicted an RD of 4.88 (4.35–5.40). As reference, dashed line shows RD of 1 for a single mixed compartment.

cally plausible on the basis of our measured tissue lipid contents. However, our observed mean residence times were twice as long as those predicted by the model. Recalculating the residence times with the λ values held constant at published values of 0.68 (17) for muscle and 0.87 for subcutaneous tissue (10) gives observed means that are on average 2.5 times longer than the predicted means.

How large would the tissue-blood partition coefficients have to be to account for the observed mean residence times by use of the present model? Setting *Eq. 5* equal to the observed mean residence time and solving for an average λ for the tissue, we estimate that the partition coefficients would have to be 2.2 for the isolated muscle and 3.2 for the intact side. Both of these values are considerably larger than any of the reported coefficients for these tissues (10, 17). Alternatively, using *Eq. 5* with the average published λ values, we can estimate the amounts of lipid that would be required to explain the observed mean residence times: 16.5% for the isolated muscle and 27.5% for the intact side. Again, these greatly exceed our measured lipid fractions as well as those reported in the literature (4, 8).

Dispersion of Residence Times

The results shown in Fig. 3 suggest that lipid contributes significantly to the RD of Xe residence times. The observed RDs are larger than can be accounted for by perfusion heterogeneity but are smaller than the predicted RDs when the compartments include lipid. What would be the effect of diffusion of gas between regions? Computer simulations show that increasing the diffusion between heterogeneous features such as lipid and nonlipid tissues diminishes the RD (5). This suggests that a strict compartmental representation of inert gas exchange is unrealistic, because it fails to account for the effects of diffusion.

Considerations

Because our results are not explained by a model using physiologically plausible parameter values, we must consider potential errors in the data measurement and in the model itself.

Error in measured blood flow rate. During 5-h experiments, do four blood flow measurements adequately represent the tissue blood flow, compared with the hundreds of data points of the Xe curves? If the tissue blood flow rates during the intervals between microsphere injections were actually half as large as those found by our measurements, our biased high flow averages would predict inappropriately short mean residence times. Analyzing the variability of the measured flows, we find that the 95% confidence intervals are within one-third of the mean flows of the four sampled values.

Could smaller pieces of tissue contain sufficiently large flow heterogeneities to explain the observed Xe RDs? Previous measurements (12) on 280-mg tissue pieces, one-fourth the size of those measured here, found even less flow heterogeneity (RD = 1.10) than in the ~1-g pieces measured here. Diffusional mixing largely obscures flow heterogeneity influences in this size range (6).

Error in detector-tissue representation. We did not determine the relative position of each tissue piece in the field of view of the Xe detector. What would the predicted mean residence time be if all the slowly exchanging pieces were located near the detector and therefore contributed disproportionately to the recorded Xe signal? Using the APPENDIX to recalculate the predicted mean residence times under these circumstances, we find that the ratio of observed to predicted mean residence times decreases from 2.2 to 1.8 for the isolated muscle and from 1.7 to 1.4 for the intact side. So even our most conservative consideration of the lipid and the detector-tissue geometry still leaves a discrepancy between the observed Xe mean residence times and the predictions of the model.

Conclusions

The results presented here demonstrate that a multiple-compartment model does not accurately describe Xe gas exchange in tissue. Plausible values for the tissue-blood partition coefficients and the lipid contents of the tissues do not explain the observed means and RDs of Xe residence times. Recirculation of Xe in the tissue by countercurrent vessel exchange or other diffusion-based processes may be important. Experiments considering

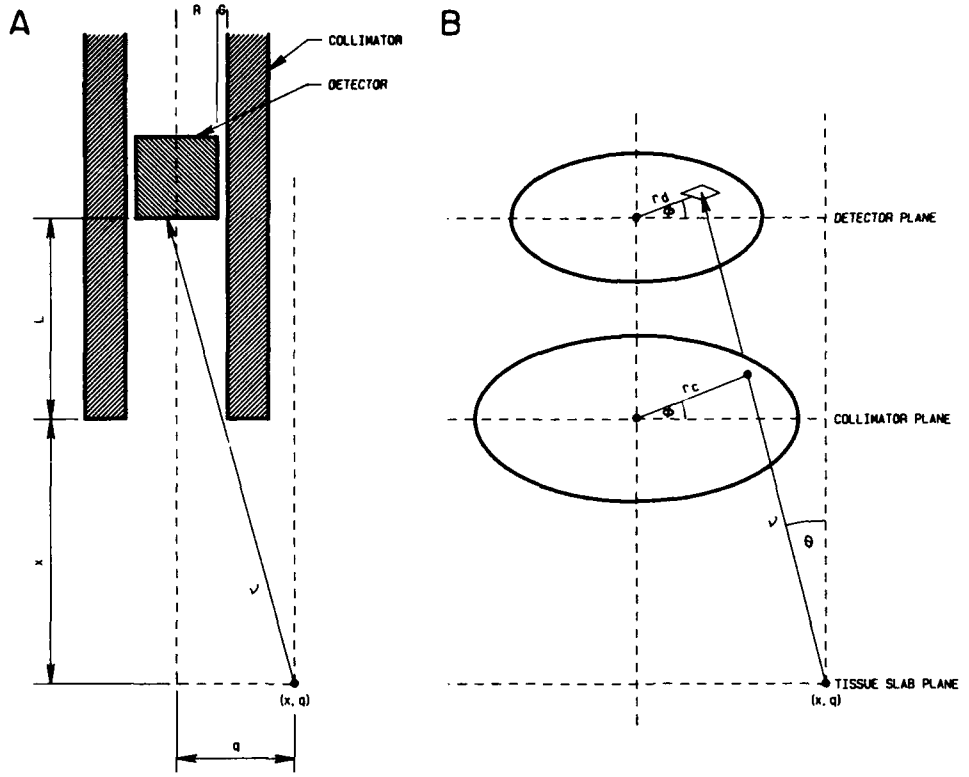

FIG. 4. *A*: schematic showing cross section of detector-collimator positioned above tissue slab. Total radioactivity detected from a point at (x,q) is calculated by integrating detector surface over (r,ϕ) for all vectors ν. *B*: detector view is established by constraints of collimator edges in plane of collimator. See text for definitions of abbreviations.

gas diffusivity and tissue architecture are needed to evaluate these notions.

APPENDIX

Model of Tissue-Detector Geometry

To estimate the fraction of radioactivity contributed by a tissue layer of variable thickness and distance from the detector, we approximate the tissue as a slab with a uniform density of radioactivity. A detector with a circular surface of radius R and area A is positioned above and normal to the slab surface (Fig. 4). The detector shaft is housed in a collimator that extends length (L) beyond the detector tip, with a small gap (G) between the detector and the collimator interior. The collimator tip rests against the slab surface at $x = 0$, where x is the distance into the slab. The collimator establishes a conical view of the slab and allows no radioactivity to penetrate its walls. The distance q extends radially in the plane of the slab normal to the cone axis.

A point at (x,q) establishes a vector (ν) of radioactivity to a small area (dA) of the detector surface at (r_d,ϕ). The efficiency of detection of a given point depends on three factors: the radial location in the slab plane, the distance from the detector, and the attenuation of the radioactivity by the tissue. First, the radial location, a point at (x,q), is detected with an efficiency proportional to $\cos\theta$, where $\cos\theta = (x + L)/\nu$. That is, points directly in front of the detector surface (toward $\cos 0 = 1$) are detected more efficiently than those to either side (toward $\cos \pi/2 = 0$). Second, the distance, the detected radioactivity, falls off as the inverse of the square of ν, as if the point were on the surface of a sphere of area $4\pi\nu^2$. The detected activity (dE) as a function of radial location and distance is expressed as

$$dE = \frac{\cos\theta dA}{4\pi\nu^2} \qquad (A1)$$

Third, the tissue attenuates the radiation traveling through it (14). This is expressed as

$$dE_{(x,q)} = \exp(-a\nu')dE \qquad (A2)$$

where a is the linear attenuation coefficient (in units of reciprocal distance) and $\nu' = \nu - (L/\cos\theta)$ is the distance traveled through the tissue.

The sum E of the detected radioactivity at the detector surface from radiation at any point (x,q) is then expressed as

$$E_{(x,q)} = \int_0^{\pi}\int_0^{R_d} \frac{\exp(-a\nu')\cos\theta r_d}{4\pi\nu^2} dr_d d\phi \qquad (A3)$$

where

$$\nu^2 = r_d^2 + q^2 - 2r_d q\cos\phi + (x + L)^2 \qquad (A4)$$

and

$$r_c \le R + G \qquad (A5)$$

Equation A5 means that only vectors within the collimator view are counted at the detector surface.

Equation A3 solved by numerical integration allows us to calculate the radioactivity detected from any point in the slab. Integrating over depth x, radius q, and angle θ in the plane of the slab shows that all planes contribute equally, because the enlargement of the detector view perfectly offsets the decline in radioactivity with distance. The attenuation due to the tissue itself, however, causes the nearer layers to contribute slightly more than the farther ones. All that is required to calculate the contribution of a given layer is information about its thickness and its distance from the detector surface, which is provided by the tissue layer measurements described in METHODS. The small 1-g pieces making up any one layer of muscle or nonmuscle tissue are considered without regard to their relative positions within the layer.

The fraction of detected Xe counts (δ) coming from the nonmuscle layer of the intact side is calculated as the sum of the radioactivity corresponding to the measured thickness divided by the total radioactivity detected.

This study would not have been possible without the skill and hard work of D. R. Laws and D. R. Lacaze. We thank Janet A. Novotny for mathematical assistance; A. L. Harabin, D. M. Stevens, C. B. Sajonia, and E. D. Thalmann for helpful reviews; S. Cecire and J. Gaines for editorial assistance; and W. S. Hilleary and J. W. Morris for the illustrations.

This work was supported by Naval Medical Research and Development Command Work Unit 62233N MM33P30.004-1050.

The opinions or assertions contained herein are the private ones of the authors and are not to be construed as official or reflecting the views of the Navy Department or the naval service at large.

Present address and address for reprint requests: J. A. Novotny, 345 West 88th St. Box 2E, New York, NY 10024.

Received 13 June 1991; accepted in final form 20 November 1992.

REFERENCES

1. BLIGH, E. G., AND W. J. DYER. A rapid method of total lipid extraction and purification. *Can. J. Biochem. Physiol.* 37: 911–917, 1959.
2. CERRETELLI, P., C. MARCONI, D. PENDERGAST, M. MEYER, N. HEISLER, AND J. PIIPER. Blood flow in exercising muscles by xenon clearance and by microsphere trapping. *J. Appl. Physiol.* 56: 24–30, 1984.
3. FARHI, L. E., AND T. YOKOYAMA. Effects of ventilation-perfusion inequality on elimination of inert gases. *Respir. Physiol.* 3: 12–20, 1967.
4. FROBERG, S. O. Determination of muscle lipids. *Biochim. Biophys. Acta* 144: 83–93, 1967.
5. HOMER, L. D., AND J. A. NOVOTNY. Computer simulation of inert gas washout (Abstract). *FASEB J.* 5: A1754, 1991.
6. HOMER, L. D., P. K. WEATHERSBY, AND S. SURVANSHI. How countercurrent blood flow and uneven perfusion affect the motion of inert gas. *J. Appl. Physiol.* 69: 162–170, 1990.
7. KJELLMER, I., I. LINDBJERG, I. PREROVSKY, AND H. TONNESEN. The relation between blood flow in an isolated muscle measured with ^{133}Xe clearance and a direct recording technique. *Acta Physiol. Scand.* 69: 69–78, 1967.
8. LINDBJERG, I. F., A. M. ANDERSEN, O. MUNCK, AND M. JURGENSEN. The fat content of leg muscles and its influence on the xenon-133 clearance method of blood-flow measurement. *Scand. J. Clin. Lab. Invest.* 18: 525–534, 1966.
9. MARCUS, M. L., C. J. BISCHOF, AND D. D. HEISTAD. Comparison of microsphere and xenon-133 clearance method in measuring skeletal muscle and cerebral blood flow. *Circ. Res.* 48: 748–761, 1981.
10. MIDTGARD, U., J. HALES, A. FAWCETT, AND P. SEJRSEN. Skin blood flow in sheep: comparison of xenon-133 washout and radioactive microsphere techniques. *J. Appl. Physiol.* 63: 962–968, 1987.
11. MORALES, M. F., E. N. RATHBUN, R. E. SMITH, AND N. PACE. Studies on body composition. *J. Biol. Chem.* 158: 677–684, 1945.
12. NOVOTNY, J. A., D. L. MAYERS, Y. J. PARSONS, S. S. SURVANSHI, P. K. WEATHERSBY, AND L. D. HOMER. Xenon kinetics in muscle are not explained by a model of parallel perfusion-limited compartments. *J. Appl. Physiol.* 68: 876–890, 1990.
13. PERL, W., H. RACKOW, E. SALANITRE, G. L. WOLF, AND R. M. EPSTEIN. Intertissue diffusion effect for inert fat-soluble gases. *J. Appl. Physiol.* 20: 621–627, 1965.
14. SORENSON, J. A., AND M. E. PHELPS. *Physics in Nuclear Medicine.* New York: Grune & Stratton, 1980, p. 158, 383.
15. TONNESEN, H., AND P. SEJRSEN. Inert gas diffusion method for measurement of blood flow: comparison of bolus injection to directly measured blood flow in the isolated gastrocnemius muscle. *Circ. Res.* 20: 552–564, 1967.
16. WEATHERSBY, P. K., K. G. MENDENHALL, E. E. P. BARNARD, L. D. HOMER, S. SURVANSHI, AND F. VIERAS. Distribution of xenon gas exchange rates in dogs. *J. Appl. Physiol.* 50: 1325–1336, 1981.
17. WEATHERSBY, P. K., AND L. D. HOMER. Solubility of inert gases in biological fluids and tissues: a review. *Undersea Biomed. Res.* 7: 277–296, 1980.